Science and Technology of Advanced Materials

ISSN: 1468-6996 (Print) 1878-5514 (Online) Journal homepage: http://www.tandfonline.com/loi/tsta20

Structure and magnetic properties of Co/CoO and Co/Si core–shell cluster assemblies prepared via gas-phase

Kenji Sumiyama, Takehiko Hihara, Dong Liang Peng & Ryoji Katoh

To cite this article: Kenji Sumiyama, Takehiko Hihara, Dong Liang Peng & Ryoji Katoh (2005) Structure and magnetic properties of Co/CoO and Co/Si core–shell cluster assemblies prepared via gas-phase, Science and Technology of Advanced Materials, 6:1, 18-26, DOI: 10.1016/j.stam.2004.07.001

To link to this article: https://doi.org/10.1016/j.stam.2004.07.001

Published online: 15 Dec 2004.

ELSEVIER

Science and Technology of Advanced Materials 6 (2005) 18–26

SCIENCE AND TECHNOLOGY OF ADVANCED MATERIALS

www.elsevier.com/locate/stam

Structure and magnetic properties of Co/CoO and Co/Si core–shell cluster assemblies prepared via gas-phase

Kenji Sumiyama*, Takehiko Hihara, Dong Liang Peng, Ryoji Katoh

Department of Materials Science and Engineering, Nagoya Institute of Technology, Nagoya 466-8555, Japan

Received 21 April 2004; revised 4 June 2004; accepted 15 June 2004
Available online 25 December 2004

Abstract

Plasma-gas condensation cluster deposition systems have been introduced and applied for preparation of Co/CoO and Co/Si clusters assemblies. In Co/CoO cluster assemblies prepared by the single source PGC system with introduction of O_2 gas into the deposition chamber, fcc Co cores are covered with NaCl type CoO shells, showing marked enhancement of unidirectional and uniaxial magnetic anisotropy and a clear cross-over phenomenon in the magnetic relaxation from the high temperature thermal regime to the low temperarure quantum tunneling regime. In Co/Si cluster assemblies prepared by the double source PGC system, fcc Co cores are also covered with amorphous Si rich shells, showing rather small magnetic coercivity. Since Co/CoO and Co/Si core–shell clusters are stable in ambient atmosphere, they will be used as building blocks for novel nano-structure-controlled materials.

Keywords: Cobalt/cobalt oxide cluster; Cobalt/silicon cluster; Core–shell cluster; Electron microscopy; Magnetization; Magnetic coercivity; Macroscopic quantum tunnelling

Contents

1. Introduction

Nano-scale-heterogeneous materials have been well-known for their excellent functional properties in comparison with uniform (defect-less single crystalline) materials

* Corresponding author. Tel.: +81 52 735 5124; fax: +81 52 735 5258.
E-mail address: sumiyama@nitech.ac.jp (K. Sumiyama).

1468-6996/$ - see front matter © 2004 Elsevier Ltd. All rights reserved.
doi:10.1016/j.stam.2004.06.003

and homogeneous (amorphous or disordered) ones [1,2]. These materials have been mainly realized by quenching and annealing procedures: nanometer scale compositional and structural fluctuations have been obtained as precipitates from supersaturated solid solution produced by vapor, liquid- or solid-quenching. These procedures are versatile and appropriate for mass-production, however, the chemistry and structure of materials cannot be well-controlled because the precipitated regions leave compositionally depleted regions in their neighborhoods and inclusion of chemical impurity: their size and internal distance cannot be adjusted independently owing to the simple materials balance and mixing entropy effects. In order to overcome such restriction in semiconductor and magnetic devices technologies, several fascinating methods have been applied: nanoscale vapor deposition controls for artificial superlattice films, electron beam lithography and forcused ion beam techniques for nano-scale dots and low dimensional arrays, usage of scanning tunneling electron microscope tips for atomic scale dots and lines, etc.

In this context, nanometer-sized clusters can be used as building blocks of unique materials tailored chemically and/or physically on the nanometer scale [3,4]. Nanocrystalline materials were first proposed as assemblies of nanosize particles synthesized by gas condensation and mechanical compaction [5]. Since grain boundaries and interfaces possess different atomic environments, lack of long-range order, softening of lattice vibration and low coordination number in contrast the conventional polycrystalline counterparts prepared by melt and solidification, we can expect anomalous mechanical, electrical, and magnetic properties in nanocrystalline materials.

Moreover, nano-clusters reveal size-dependent characteristics such as quantum confinement and surface effects, and preparation of regular size clusters is very important and prevention of surface oxidation and inter-cluster aggregation are requisite. There have been two main synthetic routes for well-monodispersive size cluters, gas phase syntheses and liquid phase (or colloidal) syntheses. The formers using clean inert gas atmosphere are appropriate for laboratory scale production [6,7], while the latter using chemical solutions and surfactants are mass-productive and often give a self-organized cluster assemblies [8]. In this review article, we describe our recent experimental results based upon gas phase syntheses. We deal with first a plasma-gas-condensation cluster deposition system, second Co/CoO core–shell cluster assemblies and third Co/Si core shell cluster assemblies. We also give our perspective for the application of cluster assemblies.

2. Plasma-gas condensation method

Fig. 1 schematically describes the plasma-gas-condensation cluster deposition (PGCD) system [9,10], which we have used for preparing transition metal and alloy clusters.

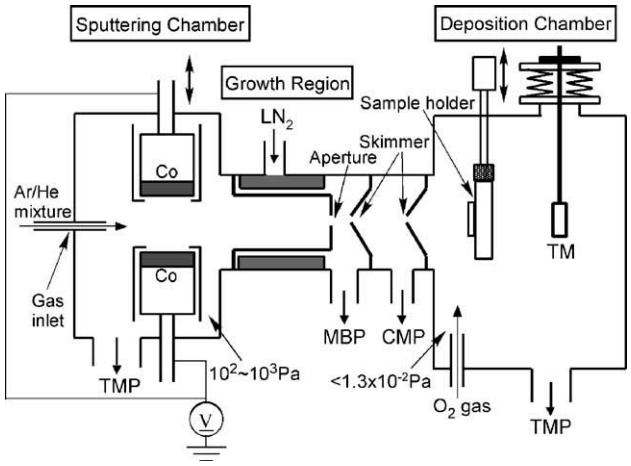

Fig. 1. A single source plasma-gas-condensation cluster deposition system [10].

The system consists of a sputtering chamber, a growth chamber and a deposition chamber. After evacuating the whole system down to 10^{-6} Pa, we inject a large amount of Ar gas. The partial Ar gas pressure of the sputtering chamber is about 100 Pa with a mechanical booster pump through a small nozzle and that of the deposition chamber in an order of 10^{-3} Pa by differential pumping and using turbo molecular pumps, where the Ar gas flow rate, R_{Ar}, is adjusted between 1.7×10^{-6} and 3.4×10^{-6} m^3/s corresponding to the Ar gas pressure, P_{Ar} between 100 and 600 Pa. Sputtered atoms collide with densely distributed Ar atoms, lose their kinetic energy and meet each other. They form a molecule if Ar atoms remove its cohesive energy [6]. A simple calculation indicates that the cluster formation process is dominated by absorption of sputtered atoms by larger cluster nuclei [11]. The deposition rate of clusters can be estimated as an effective thickness, t, by a quartz oscillation thickness monitor (TM) set near the substrate holder.

With varying the Ar gas pressure, Ar gas flow rate, sputtering power, etc. we tried to deposit clusters on transmission electron microscope (TEM) microgrids placed on the sample holder [12]. We also deposited clusters on microgrids set in the sputtering chamber, and at the entrance and exit of the growth chamber. The systematic TEM observation yields the following requisite conditions of monodispersive size clusters: the cluster nucleation must be terminated in the initial stage (in the limited space and time) and the initially nucleated clusters must be grown without further nucleation. Using this single plasma-gas-deposition system, we obtained monodispersive size transition metal clusters: the mean diameters (d) range from 5 to 15 nm with the standard deviation of size distribution was less than 10%. The high resolution TEM observation indicated well-ordered lattice images, i.e. formation of single crystal-like clusters [13]. With increasing the deposition time of such clusters on a substrate, only the number of clusters increased while their intact sizes were maintained. We clearly observed geometrical, electrical and magnetic percolation phenomena at

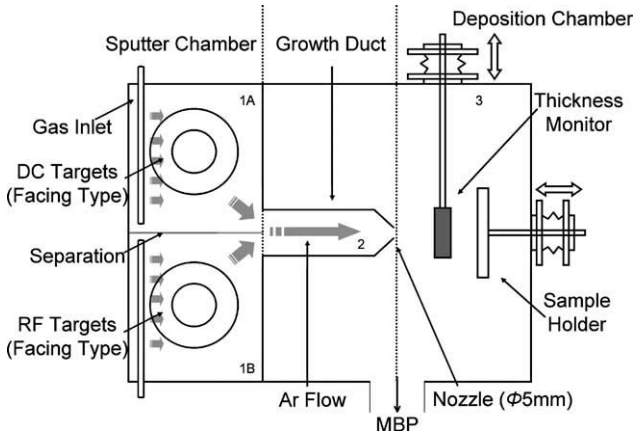

Fig. 2. A double source plasma-gas-condensation system [20].

a certain critical deposition thickness [14]. The scanning electron microscope observation indicated that thick cluster assembled films were sooty, having porous morphology [15]. Setting two different targets face-to-face in one sputtering chamber, alloy clusters could be obtained [16–19]. By applying electric powers independently to these targets, the alloy composition was adjusted and the compositional fluctuation between clusters was less than 10%.

Fig. 2 describes the two source plasma-gas-condensation system, where one cluster source is operated with a dc glow discharge mode for preparing metal clusters and another with an rf glow discharge mode for preparing semiconductor and insulator clusters [20]. Sputter (glow discharge) chambers 1A and 1B and a deposition chamber 3 are separated by the air-tight wall and indirectly connected via growth duct 2. A separation plate can be placed and removed between chambers 1A and 1B, where the vacuum conditions of both chambers are almost same. A large amount of Ar gas is introduced through gas-inlets with variable leak valves whereas chambers 1A, 1B, and duct 2 are evacuated via chamber 3 by a mechanical booster pump (500 m^3/h) to eject the Ar gas and formed clusters.

3. Co/CoO core–shell cluster assemblies

Since small clusters are so active to be easily oxidized in ambient atmosphere [21] and so unstable to coalescence each other and loose their initial sizes [22], we tried to form thin oxide layers on Co cluster surfaces with introduction of a small amount of oxygen gas into the deposition chamber (see Fig. 1) [23–25]. The cluster assemblies thus obtained are stable in ambient atmosphere. The high resolution TEM image shown in Fig. 3 indicates that a dark contrast core is covered with light contrast shells. The cross-fringes of the core region are allotted to the lattice spacings of fcc Co and those of small crystalline shell region to the lattice spacings of NaCl type CoO. The electron diffraction pattern also indicated coexistence of fcc Co and NaCl type CoO phases.

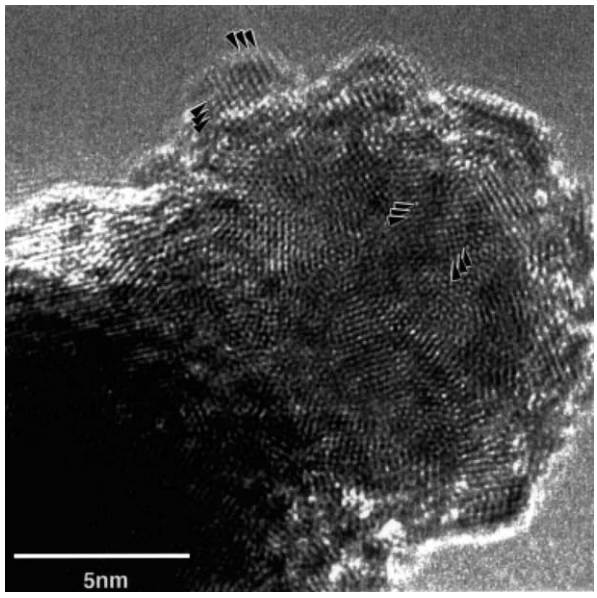

Fig. 3. A high resolution transmission microscope image of Co/CoO core–shell cluster prepared at the O_2 flow rate of 7×10^{-9} m^3/s [24]. The arrowed cross-fringes indicate the lattice spacings of fcc Co and NaCl type CoO phases.

As shown in Fig. 4, the magnetization curves at 5 K for Co/CoO core–shell clusters prepared at the O_2 flow rate $R_{O_2}=1.7\times10^{-8}$ m^3/s are different in the field cooled and non-field cooled states [23,25]. This asymmetric magnetization curve in the field-cooled state has been well-known as unidirectional anisotropy or exchange anisotropy, originating from the strong magnetic coupling between ferromagnetic Co core and antiferromagnetic CoO layers. In an external magnetic field, H, the magnetic moment of ferromagnetic cores does not easily align along H, because the antiferromagnetic CoO layers do not well-respond to H. As also shown in Fig. 5, the asymmetric

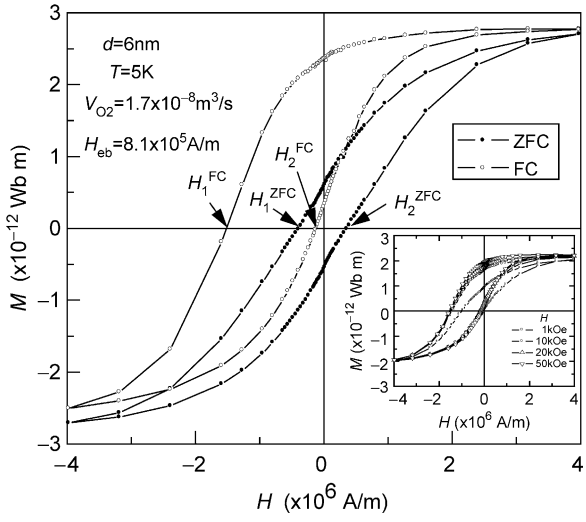

Fig. 4. Magnetization curves at 5 K for the zero-field-cooled (ZFC) and field-cooled (FC) Co/CoO core–shell cluster assemblies with the mean cluster size $d=6$ nm [25].

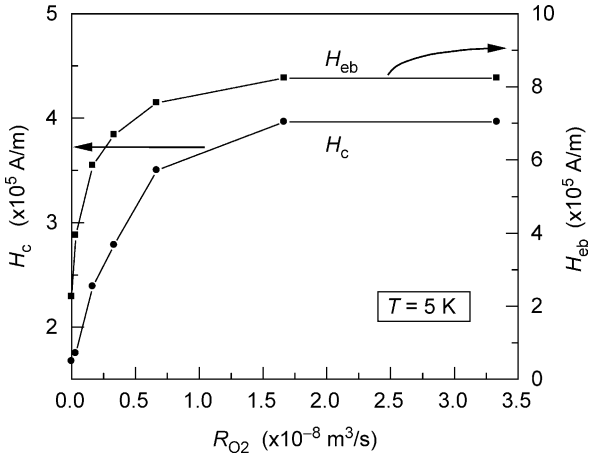

Fig. 5. Magnetic coercivity, H_c, and exchange bias field, H_{eb}, at 5 K as a function of the O_2 flow rate for Co/CoO core–shell cluster assemblies with the mean cluster size $d=6$ nm [25].

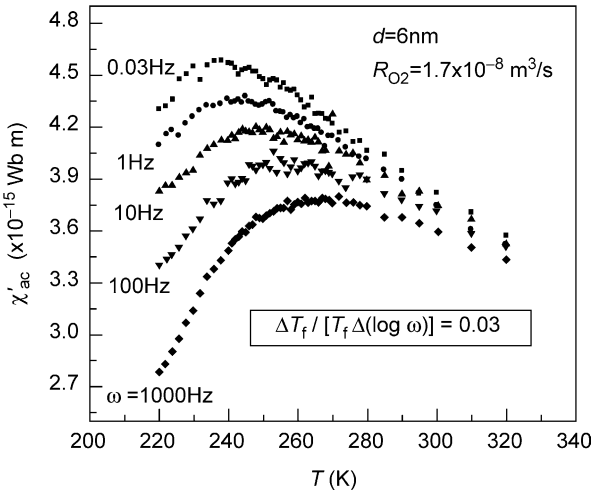

Fig. 7. Zero-field ac-susceptibility, χ' as a function of temperature, T, for Co/CoO cluster assembly with the mean cluster size of 6 nm [27].

behavior is enhanced with H and saturated above a certain high H value.

Fig. 5 shows the effect of R_{O_2} on H_c and H_{eb} for the Co/CoO cluster assemblies [25]. H_c and H_{eb} increases with increasing R_{O_2} ($<1.7\times10^{-8}$ m^3/s) and then becomes unchanged for $R_{O_2}>1.7\times10^{-8}$ m^3/s, probably because the oxidation is decelerated and reaches a stable state in the low O_2 pressure atmosphere ($<3\times10^{-4}$ Torr). The increases of H_c and H_{eb} are attributable to the increase of the exchange interaction between the ferromagnetic Co cores and antiferromagnetic CoO shells because their volume fractions change with R_{O_2}. Moreover, it should be noted that H_c rapidly increases with increasing R_{O_2}, being up to about 400 kA/m at $R_{O_2}\geq1.7\times10^{-8}$ m^3/s. This H_c value is much larger than that of Ag-coated Co particles (40–160 kA/m for $d=5$–13 nm) [15,26]. These results

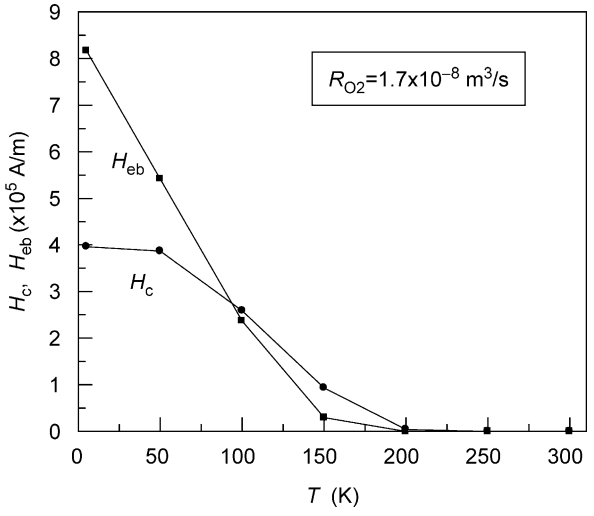

Fig. 6. Magnetic coercivity, H_c, and exchange bias field, H_{eb}, at 5 K as a function of temperature, T, for Co/CoO core–shell cluster assemblies with the mean cluster size $d=6$ nm [25].

indicate that the uniaxial anisotropy is enhanced by the exchange interaction.

Fig. 6 show H_c and H_{eb} as a function of temperature for the Co/CoO cluster assemblies prepared at $R_{O_2}=1.7\times10^{-8}$ m^3/s. H_c does not change markedly at low temperature and then decreases rapidly with increasing temperature above 100 K, while H_{eb} rapidly decreases with increasing temperature and becomes undetectable above $T_v=200$ K, where T_v is much lower than the Néel temperature ($T_N=293$ K) of the bulk CoO. The temperature dependence of H_{eb} indicates that exchange anisotropy disappears at about 200 K. A similar result observed for oxide passivated Co fine particles was attributed to the superparamagnetic behavior of the antiferromagnetic oxide shell with very small crystallites above a blocking temperature (150 K) [26]. The superparamagnetism of small antiferromagnetic particles is associated with uncompensated surface spin. However, taking into account of the roughness of core–shell interfaces as well as the small sizes of the Co cores and CoO shell crystallites, the disappearance of the loop shift above 200 K for the CoO-coated Co cluster assemblies should be due to spin disorder at and near core–shell interface. This results in the strong temperature dependence of the anisotropy for the interfacial layer of the antiferromagnetic CoO. The ac susceptibility shown in Fig. 7 strongly supports the presence of spin-glass magnetic structures at the interfaces between Co cores and CoO shells [27], inducing random anisotropy.

Magnetic relaxation measurements were performed for the Co/CoO cluster assembly using the following procedure [25]: the sample was cooled from 300 K to a lower temperature in low magnetic field, $H=8$ kA/m; the field was then reversed to $H=-8$ kA/m and the variation of the magnetization with time, t, was measured at this temperature. There is no single exponential time dependence as expected for a collection of identical, noninteracting single domain clusters aligned in the same direction by H (i.e. the anisotropy energy barrier is universal throughout

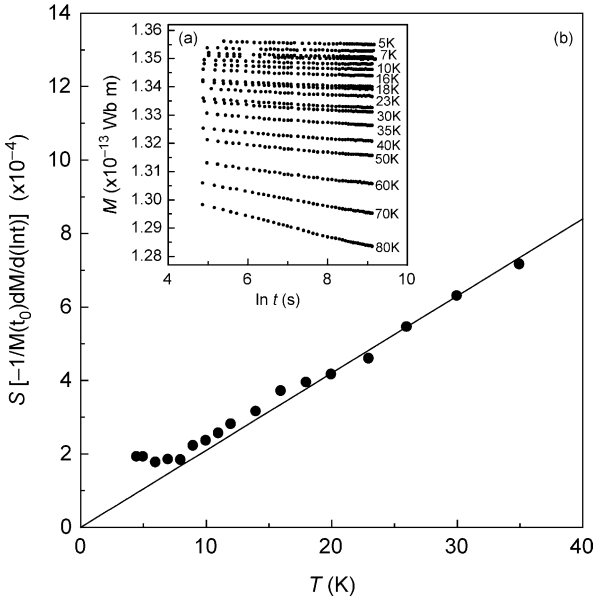

Fig. 8. (a)Time dependence of magnetization at different temperatures for Co/CoO cluster assembly with the mean cluster size $d=6$ nm [25]. (b) Temperature dependence of magnetic viscosity, $S=-1/M(t_0)\cdot[-dM(t)/d\ln t]$, for Co/CoO core–shell cluster assemblies with the mean cluster size $d=6$ nm. $M(t_0)$ and $M(t)$ are magnetizations at times t_0 and t ($t>t_0$) [25].

the system) [28]. As shown in Fig. 8(a), the magnetic relaxation obeys the following logarithmic time dependence [25,28]:

$$M(t) = M(t_0)[1 - S(T)\ln(t/t_0)] \quad (1)$$

where S is the magnetic viscosity and t_0 the fitting parameter. This implies a wide distribution of the anisotropy energy which is ascribed to the polycrystalline CoO and different interfacial state in spite of the narrow cluster size distribution. By least square fitting of eq (1) to the results in Fig. 8(a), the S value is estimated as a function of temperature and shown in Fig. 8(b). For $T>8$ K, S varies linearly with T, extrapolating to zero when $T=0$, as would be expected for the magnetic relaxation via thermal activation. This indicates that the interaction between the Co cores is smaller than the energy barrier height, probably because the dipole interaction between the Co cores is shielded partially by the antiferromagnetic CoO shells. However, the S values are independent of temperature at $T\leq 8$ K. Such a nonthermal relaxation character at very low temperatures has been observed in several nanostructured materials with the broad distribution of sizes or anisotropy energy barriers, being ascribed to a macroscopic quantum tunneling (MQT) effect of magnetization [28]. The MQT effect is observable at experimentally accessible temperatures only for materials with high uniaxial anisotropy. Indeed, for the present Co/CoO cluster assembly, $H_c=$ 400 kA/m (see Fig. 5) and the uniaxial anisotropy constant, $K\approx H_c\times M_s\approx 7.2\times 10^5$ J/m^3 which is larger than the bulk value ($K=4.5\times 10^5$ J/m^3 and 2.5×10^5 J/m^3 for bulk hcp and fcc Co, respectively and that for simple Co cluster assemblies). Therefore, the high crossover temperature (from a thermal activation regime to a quantum tunneling regime), $T_{CO}=8$ K, is ascribed to the enhanced uniaxial anisotropy due to exchange coupling between the ferromagnetic Co core and antiferromagnetic CoO shell.

4. Co/Si core–shell cluster assemblies

We prepared Co/Si composite clusters using the two source PGC system (see Fig. 2), with the rf power at 150 W and the dc power between 180 and 300 W to vary the mixing ratio of Co clusters to Si clusters, and $P_{Ar}=300$–600 Pa [20]. Fig. 9 shows the TEM image of composite clusters prepared at the dc electric powers of 250 W with inserting the separation plate between chambers 1A and 1B [29]. Here, small clusters and highly aggregated clusters are overlapped. Individual clusters could not be analyzed due to overlapping of Co and Si clusters, while the large clusters indicated as (A) and small clusters indicated as (B) were determined to be 4 at.% Co and 91 at.% Co, respectively. The sizes of separated small clusters observed as dark contrasted regions are 10–20 nm in diameter and their size distribution is much less than that of the large aggregated clusters. These results suggest that small ones are Co clusters and the large aggregates Si rich clusters. It should be mentioned that the P_{Ar} values in this session were much higher than that in section 3 (100 Pa) and thus sputtered atoms and formed clusters were prolonged to collide each other.

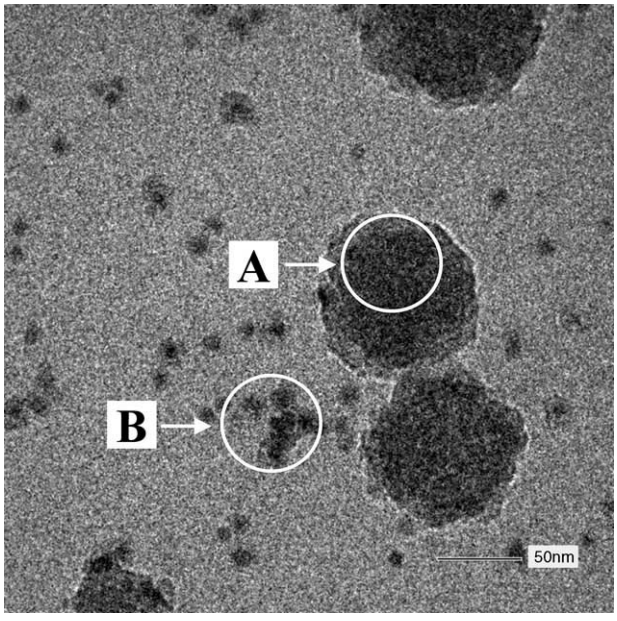

Fig. 9. Bright field TEM images of Co and Si composite clusters prepared by dc and rf glow discharge modes with inserting the separate plate between two chambers, 1A and 1B [29]. (a) the TEM image for a higher cluster density region and (b) that for a lower cluster density region, respectively. The average chemical composition of this cluster assembly is 94 at.% Co.

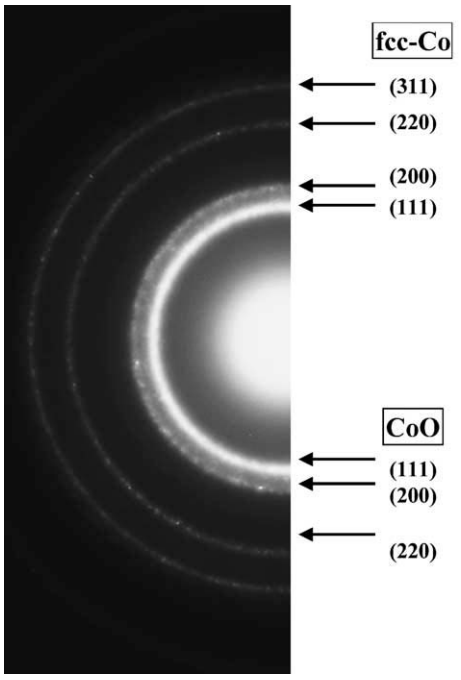

Fig. 10. A selected area electron diffraction pattern of of Co/Si composite clusters prepared by dc and rf glow discharge modes with inserting the separate plate between two chambers, 1A and 1B [29]. The average chemical composition of the cluster assemblies is 94 at.% Co by EDX analyses.

As shown in Fig. 10 [29], the diffraction pattern consists of fcc rings and broad halo rings overlapping with (111) and (200) lines of fcc Co in the Co/Si composite cluster assembly with the average composition of 72 at.% Co, being attributed to Co and Si clusters whereas weak diffraction rings corresponding to a CoO phase are also detectable. When we formed Co and Si clusters independently with inserting the separation plate between chambers 1A and 1B, the vaporized atoms and formed cluster nuclei are very quickly cooled in such a high Ar gas atmosphere, mixed in duct 2 and simultaneously deposited on the substrate. In the equilibrium phase diagram of Co–Si system [30], Co forms the primary solid solution up to 12 at.% Si at about 1000 K, while Si form almost no primary solid solution up to 1700 K. Since the Co and Si cluster sizes are also larger than the critical size of about 10 nm for occurrence of the instantaneous alloying [31], it is reasonable that fcc Co and amorphous Si clusters coexist on the substrate.

Fig. 11 shows a Co/Si composite cluster assembly (with the average composition of 22 at.% Co) prepared at the dc electric powers of 250 W without inserting the separation plate between chambers 1A and 1B [29]. As seen in this figure, the dark contrast clusters are surrounded by the gray contrast ones The average sizes of dark contrasted clusters are not uniform and rather small. The microbeam energy dispersive X-ray analysis indicated that the chemical composition of a dark core region was about 45 at.% Co and that of a gray shell region about 18 at.% Co. Fig. 12 shows the electron diffraction pattern of a Co/Si core–shell cluster assembly. It reveals diffused fcc rings (attributable to Co clusters), broad halo rings (attributable to Si clusters)

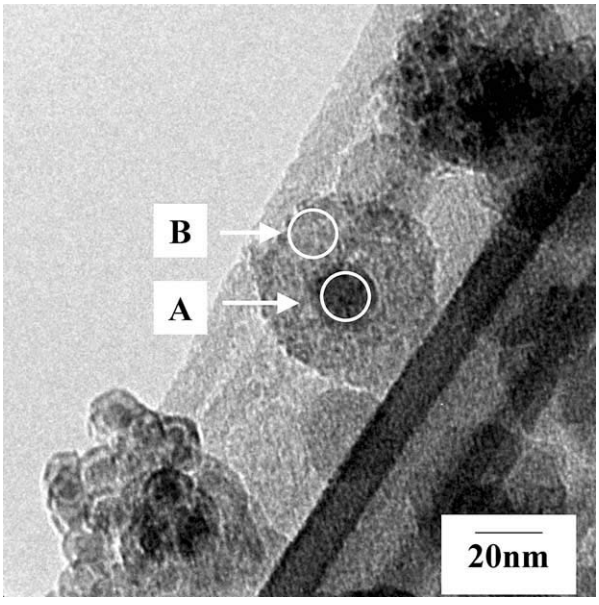

Fig. 11. Bright field TEM image and energy-dispersive X-ray analyses of Co/Si composite clusters prepared by dc and rf glow discharge modes without inserting the separate plate between two chambers, 1A and 1B [29]. The region marked by A is about 45 at.% Co and the one marked by B about 18 at.% Co, whereas the average chemical composition of these cluster assemblies is about 22 at.% Co.

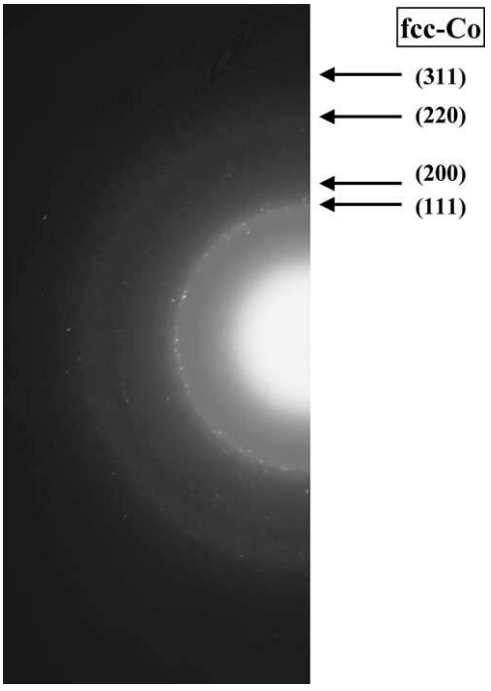

Fig. 12. A selected area electron diffraction pattern of Co/Si composite clusters deposited on a carbon micro-grid by dc and rf glow discharge modes without inserting the separate plate between two chambers, 1A and 1B [29]. The average chemical composition of the cluster assemblies is 37 at.% Co by EDX analyses.

and no diffraction ring corresponding to CoO. These results clearly demonstrate that a core–shell type structure is obtained when Co/Si composite cluster assemblies are obtained without the separation plate. When the cluster nuclei are mixed before they enter duct 2, Co and Si cluster nuclei collide each other. Since the surface tension of Si is much lower than that of Fe, Si clusters cover Fe cluster surfaces to form the core–shell clusters [32]. The core–shell cluster formation reduces coalescence and growth of Co clusters, leading to moderate size distribution of Co clusters. There seemed to be no marked mixing and alloying of Co and Si clusters though the nano-scale structural and chemical analyses could not be done due to contamination. The immiscible characters are quite different from our previous experiment in which homogeneously alloyed clusters were obtained using the single dc glow discharge mode [17–19]. In the equilibrium phase diagram [30], moreover, Co and Si form very stable intermetallic compounds, CoSi, Co_2Si and $CoSi_2$, indicating that their formation enthalpies are negative and their absolute values are so large that Co–Si alloy clusters have been expected in contrast to the present results. It has been reported that nano-scale island-like clusters on substrates were instantaneously alloyed with post-deposited atoms at ambient temperature [31] and silicides were easily formed when island-like grown Co films were deposited on a silicon substrate and annealed above 700 K [33]. In the present experiment, inter-cluster atom diffusion is suppressed and Co and Si clusters do not coalesce to form alloy clusters at their contact and/or collision events. Here, we have to take into account of the vacuum condition (0.1 Pa) of the cluster deposition chamber being about three orders of magnitude worse than the previous experiment. If chemically active Si cluster surfaces are oxidized by O_2 impurity included in Ar gas, the alloying of Si with Co should be suppressed.

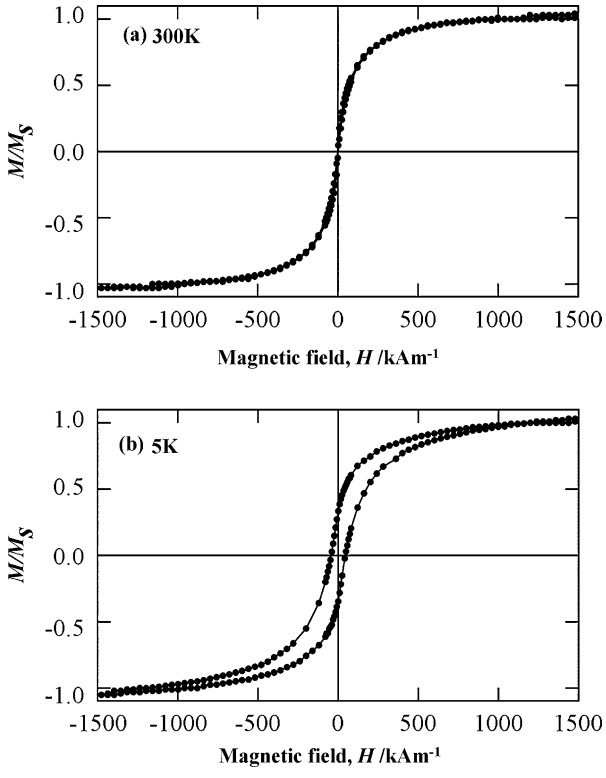

Fig. 13. Magnetization curves at (a) 300 and (b) 5 K for Co/Si composite cluster assemblies prepared without inserting the separate plate between two chambers, 1A and 1B. Its average chemical composition is 32 at.% Co [29].

Fig. 13 shows the typical magnetization curves at 300 and 5 K for Co/Si composite cluster assemblies of 37 at.% Co prepared without inserting the separation plate between chambers 1A and 1B with the dc electric power of 180 W and the rf electric power of 150 W at $R_{Ar}=2.5\times10^{-6}$ m^3/s. H_C, is about 2.4 kA/m at 300 K and about 40 kA/m at 5 K, being much smaller than those of simple Co cluster assemblies and Co/CoO core–shell cluster assemblies described in Section 3. These results suggest that the Co/Si composite cluster assemblies are not easily oxidized in ambient atmosphere.

5. Conclusion and perspective

In this article, we have introduced the plasma gas condensation method and described the two unique core–shell cluster assemblies. We also discussed structural and magnetic characteristics of Co/CoO core–shell cluster assemblies prepared by a single plasma-gas-condensation cluster-deposition system and those of Co/Si core–shell cluster assemblies prepared by a double cluster source system. Co/CoO core–shell cluster assemblies in which neat fcc Co cores are covered with NaCl type CoO crystallites reveal unidirectional anisotropy and marked enhancement of magnetic coercive force, leading to a macroscopic quantum tunneling effect in the magnetic relaxation at low temperatures. Co/Si core–shell cluster assemblies in which fcc Co cores are surrounded by small amorphous Si rich particles reveal very small magnetic coercive force, being much smaller than Co and Co/CoO cluster assemblies. These results demonstrate that core–shell clusters are very stable in ambient atmosphere and useful as building blocks of nano-scale structure controlled materials, which cannot be prepared by conventional co-evaporation or precipitation methods.

In small ferromagnetic clusters, a single domain structure is favorable due to the serious loss of domain wall energy. However, the oxidation of ferromagnetic metal cluster surfaces induces magnetic coupling between the ferromagnetic core and antiferromagnetic shell crystallites and give rise to the marked coercivity. Since T_N becomes 293 K for bulk CoO, the coercivity and thus ferromagnetism of Co clusters can be maintained even at room temperature for Co clusters embedded in continuous CoO films instead of CoO layers [34].

Now, we can prepare size-controlled clusters as building blocks and just stand on the entrance to fabricate cluster

assembled materials. We are searching new academic and industrial fields of small clusters, i.e. medical science, drug delivery, catalysis, etc. In order to assemble such small clusters without loosing their unique characteristics, the stabilization of clusters by surface coating is effective. Gas-phase syntheses using vacuum based systems can prepare impurity free and isotropic shape clusters minimizing degradation of unique properties, while liquid phase syntheses using solution and surfactant suffer from inclusion of oxygen and other impurities from surrounding environments. However, gas-phase syntheses can neither prepare periodical arrangements of clusters due to the random formation and deposition procedures nor anisotropic shape clusters due to the simple nucleation and growth processes. Liquid phase syntheses such as micro-emulsion and a colloidal reaction can give self-organized cluster lattices with the aid of surfactant interaction in the slow assembling process. Therefore, combination of gas-phase and condensed-phase syntheses is most appropriate [35] to realize size, orientation and periodicity-controlled cluster assemblies.

Acknowledgements

These works have been supported by Core Research for Evolutional Science and Technology (CREST) of the Japan Science and Technology Corporation (JST), by NITECH 21st Century COE Program 'World Ceramics Center for Environmental Harmony', by Intellectual Cluster Project of the Ministry of Education, Science, Culture and Sports, Japan, Aichi Prefecture, Nagoya City and Aichi Science and Technology Foundation, by a Grant-in-Aid for Scientific Research of the Ministry of Education, Science, Culture and Sports, Japan. We appreciate Dr S. Yamamuro, Prof T.J. Konno and Mr K. Wakoh for their helpful discussion and experimental collaboration, and Mr K. Tsunoda for his experimental assistance. One (K.S.) of the authors appreciates the support of the Research Encourage Program of Nagoya Institute of Technology and the other (D.L.P.) for the financial support from Japan Society for Promotion of Science.

References

[1] A.S. Edelstein, R.C. Cammarata (Eds.), Nanomaterials: Synthesis, Properties and Applications, Institute of Physics, Bristol, 1996.
[2] R.P. Andres, R.S. Averback, W.L. Brown, L.E. Brus, W.A. Goddard III, A. Kaldor, S.G. Louie, M. Moscovits, P.S. Peercy, S.J. Riley, E.W. Siegel, F. Spaepen, Y. Wang, Research opportunities on clusters and cluster-assembled materials—A Department of Energy, Council on Materials Science Panel Report, J. Mater. Res. 4 (1989) 704–736.
[3] R. Uyeda, Studies of ultrafine particles in Japan: Crystallography, methods of preparation and technological applications, Progr. Mat. Sci. 35 (1991) 1–96.
[4] C.G. Granqvist, R.A. Buhrman, Ultrafine metal particles, J. Appl. Phys. 47 (1976) 2200–2219.
[5] H. Gleiter, Nanocrystalline Materials, Progr. Mat. Sci. 33 (1989) 223–315.
[6] H. Haberland (Ed.), Clusters of Atoms and Molecules I and II, Springer, Berlin, 1994.
[7] P. Melinon, V. Paillard, V. Dupuis, A. Perez, P. Jensen, A. Hoareau, J.P. Perez, J. Tuaillon, M. Broyer, J.L. Vialle, M. Pellarin, B. Baguenard, J. Lerme, From free clusters to cluster-assembled materials, Int. J. Mod. Phys. B9 (1995) 339–397.
[8] C.B. Murray, D.J. Norris, M.G. Bawendi, Synthesis and characterization of nearly nonodisperse CdE (E=S,Se,Te) semiconductor nanocrystallites, J. Am. Chem. Soc. 115 (1993) 8706–8715.
[9] H. Haberland, M. Karrais, M. Malland, Y. Thurner, Thin films from energetic cluster impact: A feasibility study, J. Vac. Sci. Technol. A10 (1992) 3266–3271.
[10] S. Yamamuro, K. Sumiyama, M. Sakurai, K. Suzuki, Cr cluster deposition by plasma-gas-condensation method, Supramol. Sci. 5 (1998) 239–245.
[11] T. Hihara, K. Sumiyama, Formation and size control of a Ni cluster by plasma gas condensation, J. Appl. Phys. 84 (1998) 5270–5276.
[12] S. Yamamuro, K. Sumiyama, K. Suzuki, Monodispersed Cr cluster formation by plasma-gas-condensation, J. Appl. Phys. 85 (1999) 483–489.
[13] S. Yamamuro, K. Sumiyama, T.J. Konno, K. Suzuki, Structural and magnetic evolution in self-assembling process of nanometer-sized Co clusters, Mat. Trans. JIM 40 (1999) 1450–1455.
[14] S. Yamamuro, K. Sumiyama, T. Hihara, K. Suzuki, Geometrical and electrical percolation in nanometer-sized Co-cluster assemblies, J. Phys. Condens. Matter 11 (1999) 3247–3257.
[15] S. Yamamuro, K. Sumiyama, T. Kamiyama, K. Suzuki, Morphological and magnetic characteristics of monodispersed Co-cluster assemblies, J. Appl. Phys. 86 (1999) 5726–5732.
[16] K. Wakoh, T. Hihara, D.L. Peng, K. Sumiyama, Compositional partition in Ag–Nb alloy clusters produced by a plasma-gas-condensation cluster source, NanoStruct. Mat. 11 (2000) 1245–1251.
[17] T.J. Konno, S. Yamamuro, K. Sumiyama, Formation of ordered CoAl alloy clusters by the plasma-gas condensation technique, J. Appl. Phys. 90 (2001) 3079–3085.
[18] T.J. Konno, S. Yamamuro, K. Sumiyama, Comparative study on alloy cluster formation in Co–Al and Co–Pt systems, J. Vac. Sci. Technol. B20 (2001) 834–842.
[19] D.L. Peng, T. Hihara, K. Sumiyama, Formation and magnetic properties of Fe–Pt alloy clusters by plasma-gas condensation, Appl. Phys. Lett. 83 (2003) 350–352.
[20] R. Katoh, T. Hihara, D.L. Peng, K. Sumiyama, Composite deposition of Co and Si clusters by rf/dc plasma-gas-condensation, Appl. Phys. Lett. 82 (2003) 2688–2690.
[21] H. Sakurai, F. Itoh, H. Oike, T. Tsurui, S. Yamamuro, K. Sumiyama, T. Hihara, X-ray magnetic circular dichroism on Co monodispersive cluster assemblies, J. Phys. Condens. Matter 12 (2000) 3451–3460.
[22] P. Jensen, Growth of nanostructures by cluster deposition: experiments and simple models, Rev. Mod. Phys. 71 (1999) 1695–1735.
[23] D.L. Peng, K. Sumiyama, S. Yamamuro, T. Hihara, T.J. Konno, Preparation and magnetic properties of oxide-coated monodispersive Co cluster assembly, Phys. Stat. Sol. (a) 172 (1999) 209–216.
[24] D.L. Peng, K. Sumiyama, T.J. Konno, T. Hihara, S. Yamamuro, Characteristic transport properties of CoO-coated monodispersive Co cluster assemblies, Phys. Rev. B60 (1999) 2093–2100.
[25] D.L. Peng, K. Sumiyama, T. Hihara, S. Yamamuro, T.J. Konno, Magnetic properties of monodispersed Co/CoO clusters, Phys. Rev. B61 (2000) 3103–3109.
[26] S. Gangopadhyay, G.C. Hadjipanayis, C.M. Sorensen, K.J. Klabunde, NanoStruct. Mater. 1 (1992) 449–456.

[27] D.L. Peng, K. Sumiyama, T. Hihara, T.J. Konno, Magnetic characteristics of monodispersed Co/CoO cluster assemblies, Scripta Mater. 44 (2001) 1471–1474.
[28] J. Tejada, X.X. Zhang, E.M. Chudnovsky, Quantum relaxation in random magnets, Phys. Rev. B47 (1993) 14977–14987.
[29] R. Katoh, K. Sumiyama, T. Hihara, D.L. Peng, Composite state control and magnetic properties of cobalt and silicon cluster assemblies prepared with double plasma discharge sources, Mat. Trans. JIM, in press.
[30] T.B. Massalski, J.L. Murray, L.H. Bennett, H. Baker, L. Kacprzak, Binary Alloy Phase Diagrams, American Society of Metals, Metals Park, OH, 1986, p. 801.
[31] H. Mori, M. Komatsu, K. Takeda, H. Fujita, Spontaneous alloying of copper into gold atom clusters, Philos. Mag. Lett. 63 (1991) 173–178.
[32] F.R. de Boer, R. Boom, W.C. Mattens, A.R. Miedema, Cohesion in Metals-Transition Metal Alloys, North-Holland, Amsterdam, 1989, p. 662.
[33] C. Calandra, O. Bisi, G. Ottaviani, Electronic properties on silicon–transition metal interface compounds, Surf. Sci. Rep. 4 (1985) 271–364.
[34] V. Skumryev, S. Stoyanov, Y. Zhang, G. Hadjipanayis, D. Bivord, J. Noqués, Beating the superparamagnetic limit with exchange bias, Nature 423 (2003) 850–853.
[35] R.P. Andres, J.D. Bielefeld, J.I. Henderson, D.B. Janes, V.R. Kolagunta, C.P. Kubiak, W.J. Mahoney, R.G. Osifchin, Self-assembly of a two-dimensional superlattice of molecularly linked metal clusters, Science 273 (1996) 1690–1693.